# MR Imaging Predictors of Molecular Profile and Survival: Multi-institutional Study of the TCGA Glioblastoma Data Set[1]

David A. Gutman, MD, PhD
Lee A. D. Cooper, PhD
Scott N. Hwang, MD, PhD
Chad A. Holder, MD
JingJing Gao, PhD
Tarun D. Aurora, BS
William D. Dunn, Jr, BS
Lisa Scarpace, MS
Tom Mikkelsen, MD
Rajan Jain, MD
Max Wintermark, MD, MAS
Manal Jilwan, MD
Prashant Raghavan, MD
Erich Huang, PhD
Robert J. Clifford, PhD
Pattanasak Mongkolwat, PhD
Vladimir Kleper, BS
John Freymann, BA
Justin Kirby, BS
Pascal O. Zinn, MD
Carlos S. Moreno, PhD
Carl Jaffe, MD
Rivka Colen, MD
Daniel L. Rubin, MD, MS
Joel Saltz, MD, PhD
Adam Flanders, MD
Daniel J. Brat, MD, PhD

**Purpose:** To conduct a comprehensive analysis of radiologist-made assessments of glioblastoma (GBM) tumor size and composition by using a community-developed controlled terminology of magnetic resonance (MR) imaging visual features as they relate to genetic alterations, gene expression class, and patient survival.

**Materials and Methods:** Because all study patients had been previously deidentified by the Cancer Genome Atlas (TCGA), a publicly available data set that contains no linkage to patient identifiers and that is HIPAA compliant, no institutional review board approval was required. Presurgical MR images of 75 patients with GBM with genetic data in the TCGA portal were rated by three neuroradiologists for size, location, and tumor morphology by using a standardized feature set. Interrater agreements were analyzed by using the Krippendorff α statistic and intraclass correlation coefficient. Associations between survival, tumor size, and morphology were determined by using multivariate Cox regression models; associations between imaging features and genomics were studied by using the Fisher exact test.

**Results:** Interrater analysis showed significant agreement in terms of contrast material enhancement, nonenhancement, necrosis, edema, and size variables. Contrast-enhanced tumor volume and longest axis length of tumor were strongly associated with poor survival (respectively, hazard ratio: 8.84, $P = .0253$, and hazard ratio: 1.02, $P = .00973$), even after adjusting for Karnofsky performance score ($P = .0208$). Proneural class GBM had significantly lower levels of contrast enhancement ($P = .02$) than other subtypes, while mesenchymal GBM showed lower levels of nonenhanced tumor ($P < .01$).

**Conclusion:** This analysis demonstrates a method for consistent image feature annotation capable of reproducibly characterizing brain tumors; this study shows that radiologists' estimations of macroscopic imaging features can be combined with genetic alterations and gene expression subtypes to provide deeper insight to the underlying biologic properties of GBM subsets.



[1] From the Departments of Biomedical Informatics, 36 Eagle Row, Room 572 PAIS, Emory University Hospital, Atlanta, GA 30322 (D.A.G., L.A.D.C., S.N.W., C.A.H., J.J.G., T.D.A., W.D.D., C.S.M., J.S., D.J.B.); Hermelin Brain Tumor Center, Henry Ford Hospital, Detroit, Mich (L.S., T.M., R.J.); Department of Radiology, University of Virginia, Charlottesville, Va (M.W., M.J., P.R.); National Cancer Institute, Bethesda, Md (E.H., R.J.C.); Department of Radiology, Northwestern University, Chicago, Ill (P.M., V.K.); SAIC-Frederick Inc, Frederick, Md (J.F., J.K.); Department of Genetics, MD Anderson Cancer Center, Houston, Tex (P.O.Z.); Department of Pathology and Laboratory Medicine, Emory University, Atlanta, Ga (C.S.M., D.J.B.); Department of Radiology, Boston University School of Medicine, Boston, Mass (C.J.); Department of Radiology, Brigham & Women's Hospital, Harvard University, Boston, Mass (P.O.Z., R.C.); Department of Radiology, Thomas Jefferson University Hospital, Philadelphia, Pa (A.F.); and Department of Radiology, Stanford University, Stanford, Calif (D.L.R.). From the 2011 RSNA Annual Meeting. Received March 1, 2012; revision requested May 9; revision received August 27; accepted September 5; final version accepted November 9. **Address correspondence to** D.A.G. (e-mail: *dgutman@emory.edu*).

Glioblastoma (GBM) is a malignant primary brain tumor with a poor prognosis (median survival, 14 months) despite aggressive multimodal therapy (1–3). GBM's heterogeneous neuroimaging, pathologic, and molecular features provide opportunities for subclassification, prognostication, and the development of targeted therapies (4). Noninvasive methods for diagnosing, subtyping, and monitoring growth or response to therapy would advance the practice of neuro-oncology. While the current role of magnetic resonance (MR) imaging has been limited to establishing the initial diagnosis and to monitoring treatment response, MR imaging also has the capability of quantifying specific phenotypic imaging features of these tumors, such as the volume of the necrotic core or surrounding contrast material–enhanced rim. This suggests that capturing the imaging characteristics of GBM could provide additional parameters for cataloging these tumors.

Several imaging features have been shown to have potential prognostic value. Previous studies have modeled overall survival by using feature combinations that include preoperative tumor volume, Karnofsky performance status (KPS), involvement of eloquent brain regions, volume of the nonenhanced tumor, extent of edema, extent of resection, degree of necrosis, and degree of contrast enhancement (5–8). However, since these studies do not use consistent imaging feature descriptors, the results are difficult to compare.

In addition to prognostic information, MR imaging features may also serve as noninvasive biomarkers that could offer insight to underlying molecular pathways. A comprehensive imaging-genomic analysis performed by using quantitative MR imaging volumetrics and large-scale genetic and micro-RNA expression profiles recently demonstrated the potential for molecular subtyping based on signal intensity on fluid-attenuated inversion recovery (FLAIR) images (9).

To uncover meaningful correlations between imaging features and genomic aberrations, it is critical to measure MR features both accurately and reproducibly. Since qualitative analysis of clinical neuroimaging can be obfuscated by a lack of reproducible and validated objective measures, our study utilized a subset of a recently developed controlled terminology that incorporates the majority of the visible subjective MR imaging features associated with malignant primary brain tumors. This comprehensive feature set schema (known as VASARI, for Visually AcceSAble Rembrandt Images; *https://wiki.nci.nih.gov/display/CIP/VASARI*) was developed to normalize grading of visual/subjective MR imaging features of malignant gliomas (10). The feature set was developed by domain experts (ie, neuroradiologists) to include the majority of possible subjective MR imaging features associated with malignant primary brain tumors with a validated grading system to rate each feature. It was built on many of the observations that have been previously tested and validated in the imaging literature (5). The 30 distinct features and corresponding criteria of the VASARI were developed and validated based on a consensus opinion of a panel of eight neuroradiologists at multiple institutions with extensive experience in neuro-oncology. They are based on four cardinal imaging features of nonenhanced tumor, contrast-enhanced tumor, necrosis, and edema. Terms were grouped into general categories such as lesion location, morphology, margin, vicinity of lesion, and remote alterations. The observations were harmonized against ontologies such as

## Advances in Knowledge

- Semiquantitative assessment of glioblastoma (GBM) compartments on MR images (eg, necrosis, contrast material enhancement, edema) on the basis of a standardized feature set is predictive of overall survival.
- Molecularly defined tumor subtypes show observable differences in macroscopic appearance: Proneural tumors were associated with low levels of contrast enhancement, and mesenchymal tumors were associated with lower degrees of nonenhanced tumor relative to other subtypes.

## Implications for Patient Care

- The combination of standardized neuroimaging, pathologic, and genomic features may provide a more precise method to predict a GBM tumor's biologic behavior and be used to better predict individual patient survival.
- Refinements in the classification of GBM tumors through imaging phenotype characterization may help individualize treatment regimens for this disease.
- As volumetric assessment of GBM tumor composition is not widely available, these data suggest radiologist review of MR imaging data has adequate prognostic value and correlates with genomic biomarkers.

**Published online before print**
10.1148/radiol.13120118 **Content code:** NR

**Radiology 2013;** 267:560–569

**Abbreviations:**
CI = confidence interval
FLAIR = fluid-attenuated inversion recovery
GBM = glioblastoma
KPS = Karnofsky performance status
TCGA = the Cancer Genome Atlas

**Author contributions:**
Guarantors of integrity of entire study, D.A.G., A.F., D.J.B.; study concepts/study design or data acquisition or data analysis/interpretation, all authors; manuscript drafting or manuscript revision for important intellectual content, all authors; approval of final version of submitted manuscript, all authors; literature research, D.A.G., S.N.H., C.A.H., T.D.A., W.D.D., M.J., P.O.Z.; clinical studies, D.A.G., S.N.H., C.A.H., L.S., M.J., R.C., A.F., D.J.B.; experimental studies, D.A.G., C.A.H., L.S., R.J.C., P.M., J.F., R.C., D.J.B.; statistical analysis, D.A.G., L.A.D.C., S.N.H., J.J.G., E.H., R.J.C., V.K.; and manuscript editing, D.A.G., L.A.D.C., S.N.H., C.A.H., J.J.G., T.D.A., W.D.D., R.J., M.W., M.J., E.H., V.K., J.F., J.K., P.O.Z., C.S.M., C.J., R.C., D.L.R., J.S., A.F., D.J.B.

**Funding:**
This research was supported by the National Institutes of Health (grant HHSN261200800001E).

Conflicts of interest are listed at the end of this article.

RadLex® to ensure interoperability. By using specific guidelines and controlled vocabulary, the feature set is designed to comprehensively describe the tumor in consistent and reproducible terms. This work also demonstrates that radiologist-made measurements of these features are reproducible, clinically meaningful, and biologically relevant.

The purpose of this study was to conduct a comprehensive analysis of radiologist-made assessments of GBM tumor size and composition by using a community-developed controlled terminology of MR imaging visual features as they relate to genetic alterations, gene expression class, and patient survival.

## Materials and Methods

### Radiologic Annotation and Mark-up Process

Because patient-derived clinical, imaging, and genomic data has been previously deidentified by the Cancer Genome Atlas (TCGA), which is a publicly available data set that contains no linkage to patient identifiers, no institutional review board or Health Insurance Portability and Accountability Act approval was required for our study. Baseline MR imaging data sets for 88 GBM patients with complete survival data (24 female [mean age, 59.6 years; range, 17–84 years] and 51 male [mean age, 57.5 years; range, 14–77 years]; combined mean age, 58.2 years) were obtained from the Cancer Imaging Achive *(http://cancerimagingarchive.net/)*, an imaging portal consisting of images corresponding to TCGA ptients that were collected through an interinstitutional effort by members of Henry Ford Hospital, University of California San Francisco, MD Anderson Cancer Center, Emory University, and Thomas Jefferson University Hospital (11) for retrospective image analysis. Overall survival was defined as the number of days between the date of the initial pathologic diagnosis and time to death (or point of censure if the patient was still alive). Immediate postsurgical studies ($n$ = 8) and incomplete baseline examinations (ie, not including FLAIR images and T1-weighted images obtained before and after contrast material administration) were eliminated ($n$ = 5) leaving a total of 75 cases for analysis. All available images, as of November 2011, on the Cancer Imaging Archive portal were included in the initial analysis. Cases were reviewed between February and November 2011.

For each patient, three board-certified neuroradiologists independently reviewed axial T1-weighted MR images before and after gadolinium-based contrast material administration as well as axial T2-weighted FLAIR images. Images were viewed on a workstation (ClearCanvas, Toronto, Canada; *http://clearcanvas.com*) with an electronic case report form installed that implemented the VASARI feature set for human GBM (12–16). Each board-certified neuroradiologist (C.H., 15 years of experience; A.F., 22 years; S.H., 5 years; M.W., 6 years; P.R., 4 years; and M.J., 3 years) recorded a set of mark-ups for 26 of 30 imaging features describing the size, location, and morphology of the tumor.

For the purposes of this study, the four cardinal VASARI MR imaging features were used, plus a single measure of lesion size. This subset was chosen based on the consistent representation across patients and on the ease of segmentation. The four cardinal variables were the percentage of total abnormal tissue classified as contras- enhanced tumor, nonenhanced tumor, necrosis, and edema. These variables were visually estimated by neuroradiologists and then divided into categories (eg, 0%–5%, 6%–33%, 34%–67%, 68–95, 95%–100%) according to the VASARI guidelines. Contrast-enhanced tumor was defined as that with increased signal intensity on T1-weighted images compared with that on precontrast images. Nonenhanced tumor was defined as regions of T2-weighted image hyperintensity (less than the signal intensity of cerebrospinal fluid and edema, with corresponding T1-weighted hypointensity) that is associated with mass effect and architectural distortion, including blurring of the gray-white interface. Necrosis was defined as a region within the tumor with irregular margins that does not enhance or that showed absence of central enhancement with corresponding increased signal intensity on T2-weighted and proton density–weighted images. Edema was defined on FLAIR or T2-weighted images with signal intensity greater than that of nonenhanced tumor but lower than that of cerebrospinal fluid. A lesion size estimate was also used, which was measured as the two largest perpendicular cross-sectional diameters of T2-weighted signal intensity abnormality on a single axial image (Fig 1).

For each patient image set, the feature assessments for each tumor from each of the three neuroradiologists were collapsed into a single set consisting of a consensus value for each of the imaging features. For the ordinal tumor composition features (proportion contrast-enhanced tumor, proportion nonenhanced tumor, proportion necrosis, and proportion edema), the consensus value was equal to the category the neuroradiologists selected most frequently. Missing measurements for a particular imaging feature were ignored in the determination of the consensus value. For the quantitative lesion size measurements, the consensus value was equal to the median of the neuroradiologists' measurements.

### Interreader Agreement

We assessed the interreader agreement of each of the tumor compartment features by using the Krippendorff α statistic (17). Values close to 1 indicate high interreader agreement for that particular feature, whereas values close to 0 indicate that agreement in any two readers' measurements of that feature for the same patient is due to chance. A Krippendorff α value less than zero indicates that interreader disagreements are systematic.

Interreader agreement for the lesion size measurements was assessed by means of the intraclass correlation coefficient. The intraclass correlation coefficient of the square roots of the lesion length feature values were computed since the square root transformations made these quantities approximately normally distributed.

**Figure 1**

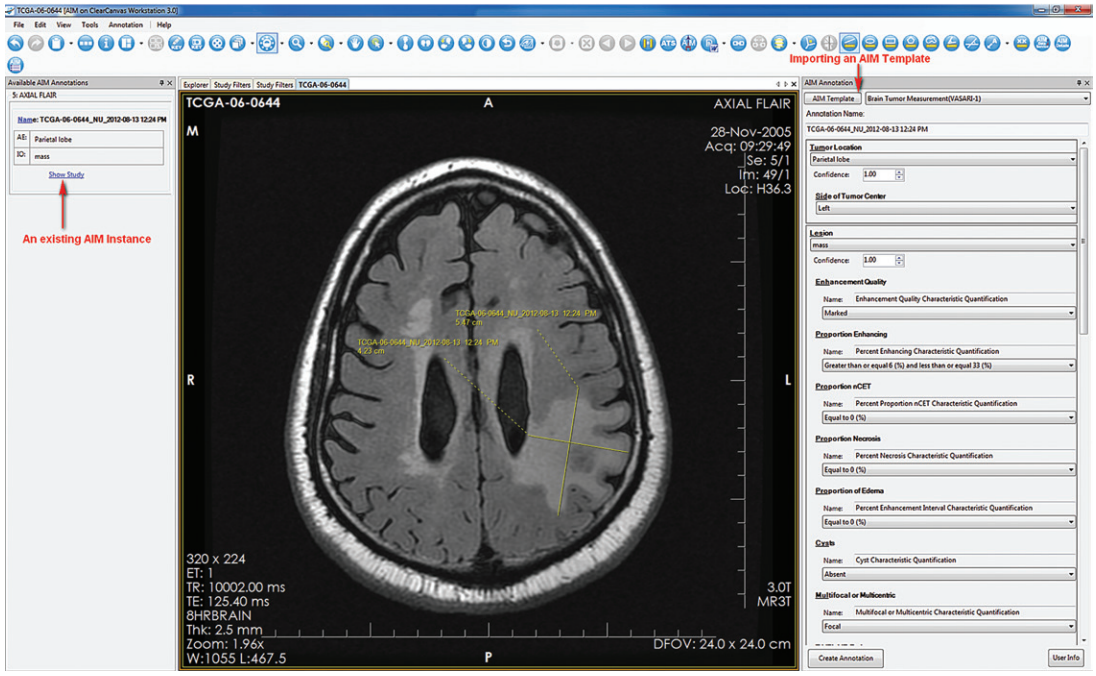


**Figure 1:** Screen shot shows an example of the Clear Canvas interface used for data entry.

### Survival and Association Analysis

Survival data representing time between initial diagnosis and death were downloaded directly from the TCGA data portal *(http://tcga-data.nci.nih.gov/tcga/tcgaHome2.jsp)*. The relationship between survival, mutation status, or molecular subtype and imaging features was addressed separately by type of image. All analyses were conducted by using either custom-written code in Matlab (Mathworks, Natick, Mass) or SAS (SAS, Cary, NC).

We examined the association between these imaging features and overall survival through Cox regression, using stepwise variable selection to determine which features to include in the model. For the purpose of this analysis, we coded the assigned ranges of values from the radiologists of each of these features as the range midpoint; we coded 0%–5% as 0.025, 6%–33% as 0.195, 34%–67% as 0.505, and so on. Seven of the 75 patients were missing overall survival outcomes; we did not use data for these patients for this analysis.

We then investigated whether any imaging features we found to be associated with overall survival in the analysis above were still associated after adjusting for standard clinical variables, including those that have previously been shown to be correlated with survival, such as KPS, age, and sex. We first performed a stepwise variable selection among the clinical variables to determine which to include in the Cox regression model. Twenty-three of the 68 patients for whom overall survival was available had missing KPS values. For all of these patients, we imputed KPS values of 80, the most commonly occurring KPS value in the data set; analyses indicated that this approach outperformed more complicated multiple imputation procedures. We then performed another stepwise variable selection among the imaging features to determine which to add to this model. We next tested the association between overall survival and any imaging features we selected in the above analysis after adjusting for the standard clinical variables by performing a likelihood ratio test of the clinical variables–plus –imaging features model versus the clinical variables–only model.

### Genetic Mutation, Genetic Expression, and Copy Number Correlations to Imaging Features

For purposes of molecular analysis, gene expression subtypes and genetic mutation status for *TP53*, *PTEN*, *EGFR*, *NF1*, and *IDH1* were obtained from supplementary material published in Verhaak et al (18). Patients were characterized into four robust gene expression classes, referred to as proneural, neural, classic, and mesenchymal as defined by a previous study by Verhaak et al (19).

Correlations between imaging features and Verhaak subtypes were calculated by using the Fisher exact test. Correlations between imaging features and mutation status of *EGFR*, *ERBB2*, *IDH1*, *NF1*, *PDGFRA*, *PIK3CA*, *PIK3R1*, *PTEN*, *RB1*, and *TP53* were evaluated by using the Fisher exact test. Owing to the heterogeneous nature of mutations and a small percentage of GBMs having mutation in any individual gene, there was not sufficient power to perform a global

**Figure 2**

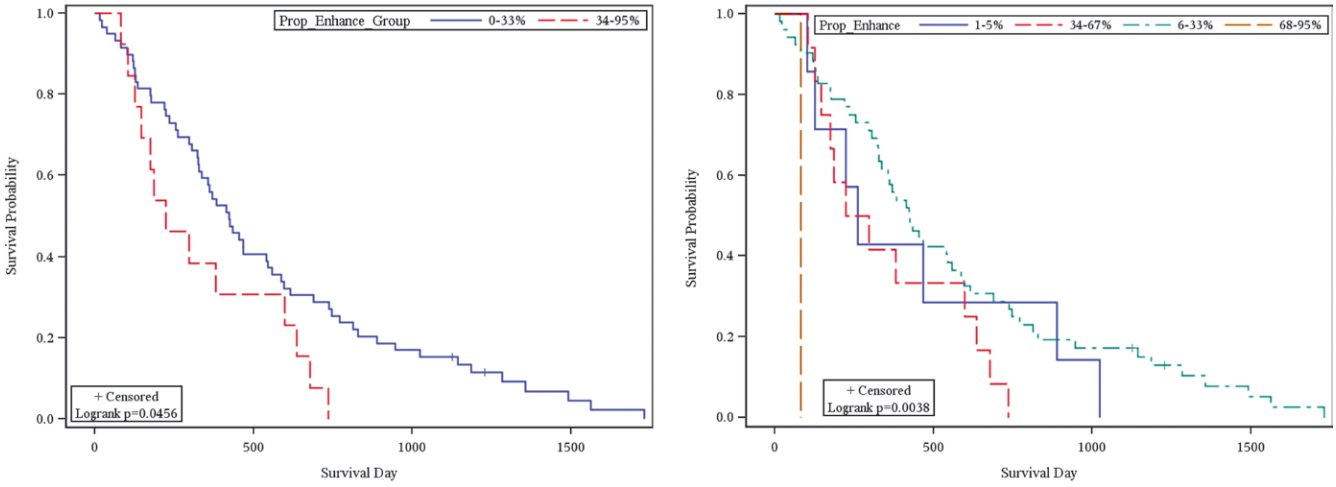


**Figure 2:** **(a)** Kaplan-Meier survival curves for comparing survival rates between two dichotomized subgroups for the feature proportion contrast-enhanced tumor. **(b)** Kaplan-Meier survival curves for comparing survival rates between all categories.

analysis. Most mutations were only present in approximately 10% of patients, limiting the number of patients with any given genotype to approximately five to 10 patients. Therefore, we instead compared specific subpopulations of patients to examine specific genotype-phenotype associations based on specific genes of interest identified in previous work (19). Multiple test-correction was performed by using the Benjamini-Hochberg correction implemented in Matlab (20).

In addition, copy number data were used to identify a subgroup of patients with high-level *EGFR* amplification, with high-level *PDGFRA* amplification, with homozygous deletions of *CDKN2A*, and with deletions of *NF1* by using data obtained from the cBio Cancer Genomics Portal (21). For copy number analysis, raw data were first converted into an ordinal ranking (homozygous deletion, heterozygous deletion, wild type, low-level amplification, high-level amplification) as described in the cBio Cancer Genomics Portal prior to correlation analysis. Copy number data were subsequently analyzed for associations/enrichment of radiology imaging features and copy number status of specific genes. Multiple test-correction was performed by using the Benjamini-Hochberg correction implemented in Matlab (20).

**Table 1**

**Hazard Ratios for Association between Imaging Features and Overall Survival**

| Variable | Hazard Ratio | *P* Value |
|---|---|---|
| KPS | 0.972 (0.953, 0.992) | .0057 |
| Major axis length | 1.016 (1.002, 1.030) | .030 |
| Proportion contrast-enhanced tumor | 7.745 (1.135, 52.87) | .037 |

Note.—Data are hazard ratio estimates, with 95% CIs in parentheses, for variables included in the Cox regression model involving imaging features plus clinical variables, for the analysis of the association between the imaging features and overall survival after adjusting for standard clinical variables. Likelihood ratio test of this model versus null model: $P = .00059$ (test statistic = 17.4 with three degrees of freedom).

## Results

### Interrater Reliability

Interreader agreements for the four cardinal imaging features were moderate to high; the tumor composition feature with the highest interreader agreement was proportion contrast-enhanced tumor ($\alpha = 0.607$; 95% confidence interval [CI]: 0.403, 0.749). Moderate agreements were also noted for the other estimates: proportion nonenhanced tumor ($\alpha = 0.428$; 95% CI: 0.239, 0.565), proportion necrosis ($\alpha = 0.511$; 95% CI: 0.358, 0.646), and proportion edema ($\alpha = 0.496$; 95% CI: 0.339, 0.608). The intraclass correlations for the two lesion size measurements were 0.647 (95% CI: 0.541, 0.753) and 0.554 (95% CI: 0.431, 0.677).

### Neuroimaging Features and Survival

The length of the lesion's major axis, based on the longest axis section at T2-weighted FLAIR imaging, and the proportion of contrast-enhanced tumor were both significantly associated with poor survival (hazard ratio: 1.02, $P = .00973$, and 8.84, $P = .0253$, respectively) (Fig 2). Overall survival was not significantly associated with the proportion of necrosis, proportion of edema, proportion of nonenhanced tumor, or length of the lesion's minor axis.

Of the three standard clinical variables we considered, only KPS was associated with overall survival (hazard ratio: 0.972, $P = .0057$; Table 1). Even when KPS was included in the Cox regression model, the length of the lesion's

**Table 2**

**Associations between Imaging Features and Verhaak Subtypes Based on Original Categoric Ranges of VASARI Feature Set**

| Neuroimaging Feature and Subtype | No. of Tumors Present of Each Subtype (Out of 70) according to Percentage of Total Abnormal Tissue | | | | *P* Value |
|---|---|---|---|---|---|
| | 0%–5% | 6%–33% | 34%–67% | 68%–95% | |
| Edema | | | | | |
| Classic | 3 (4.35) | 4 (5.8) | 9 (13.04) | 0 | .09 |
| Mesenchymal | 4 (5.8) | 8 (11.59) | 11 (15.94) | 2 (2.9) | |
| Neural | 2 (2.9) | 9 (13.04) | 3 (4.35) | 0 | |
| Proneural | 7 (10.14) | 3 (4.35) | 4 (5.8) | 0 | |
| Total | 16 (23.2) | 24 (34.8) | 27 (39.1) | 2 (2.9) | |
| Contrast-enhanced tumor | | | | | |
| Classic | 0 | 13 (18.57) | 3 (4.29) | 0 | .02 |
| Mesenchymal | 1 (1.43) | 19 (27.14) | 5 (7.14) | 0 | |
| Neural | 0 | 13 (18.57) | 2 (2.86) | 0 | |
| Proneural | 5 (7.14) | 6 (8.57) | 2 (2.86) | 1 (1.43) | |
| Total | 6 (8.6) | 51 (72.9) | 12 (17.1) | 1 (1.4) | |
| Necrotic | | | | | |
| Classic | 1 (1.43) | 13 (18.57) | 2 (2.86) | | .16 |
| Mesenchymal | 7 (10) | 13 (18.57) | 5 (7.14) | | |
| Neural | 3 (4.29) | 8 (11.43) | 4 (5.71) | | |
| Proneural | 5 (7.14) | 4 (5.71) | 5 (7.14) | | |
| Total | 16 (22.9) | 38 (54.3) | 16 (22.9) | | |
| Nonenhanced tumor | | | | | |
| Classic | 10 (14.29) | 4 (5.71) | 2 (2.86) | 0 | <.01 |
| Mesenchymal | 20 (28.57) | 4 (5.71) | 0 | 1 (1.43) | |
| Neural | 4 (5.71) | 6 (8.57) | 4 (5.71) | 1 (1.43) | |
| Proneural | 4 (5.71) | 4 (5.71) | 3 (4.29) | 3 (4.29) | |
| Total | 38 (54.3) | 18 (25.7) | 9 (12.9) | 5 (7.1) | |

Note.—Numbers in parentheses are percentages. *P* values were obtained with the Fisher exact test.

major axis and the proportion of contrast-enhanced tumor were still both significantly associated with poor survival (hazard ratio: 1.02, $P = .030$, and hazard ratio: 7.75, $P = .037$, respectively). The likelihood ratio test of the model of overall survival versus KPS alone in comparison with the model of overall survival versus KPS, length of the lesion's major axis, and proportion of contrast-enhanced tumor also indicated the significant association between overall survival and these imaging features even after adjustment for KPS ($P = .0208$).

### Neuroimaging Features and Molecular Subtype

We found a significant association between contrast-enhanced tumor and Verhaak gene expression classification ($P = .02$) (Table 2). In particular, the proneural expression class was enriched with GBMs that displayed low levels (< 5%) of contrast enhancement, whereas very few of the other three classes of GBM showed low levels (eg, < 5%) of contrast enhancement. There was also a significant association between nonenhanced tumor and expression class ($P < .01$). Similarly, the mesenchymal subtype was noted to have significantly lower rates of nonenhanced tissue compared with other tumor subtypes ($P < .01$).

### Neuroimaging Features and Mutation Status

We did not detect any significant associations between gene mutation status and specific imaging features, likely due to the relatively heterogenous nature of mutations in GBM and the small percentage of tumors having a mutation in any individual gene (Table 3).

We also found that *EGFR* mutant GBMs (10 of 49 patients with imaging data) were significantly larger based on the T2-weighted FLAIR images than wild-type *EGFR* GBMs ($P < .05$). *TP53* mutant GBMs (nine of 49 patients) were smaller than those that were wild type ($P < .006$) based on the T2-weighted FLAIR images. *EGFR* mutant GBMs ($n = 10$) were significantly larger than *TP53* mutants ($n = 9$; $P < .0005$).

### Neuroimaging Features and Copy Number Expression

Our analysis indicated that there were weak correlations between imaging features and copy number variation (Table 4). There was only weak association between *CDKN2A* deletion and necrosis ($P = .05$ uncorrected), and amplification of *EGFR* and increased percentage of contrast enhancement ($P =$

**Table 3**

**Distribution of Mutation Status according to Neuroimaging Features and Association Analysis**

| Gene and Neuroimaging Feature | No. of Tumors of Each Mutation (Out of 48) according to Percentage of Total Abnormal Tissue | | | *P* Value (Fisher Exact Test) | Benjamini-Hochberg Corrected *P* Values |
|---|---|---|---|---|---|
| | 0%–5% | 06%–33% | 34%–95% | | |
| *EGFR* | | | | | |
| Edema | 2 | 3 | 5 | .90 | >.99 |
| Contrast-enhanced tumor | 0 | 9 | 1 | .59 | .932 |
| Necrotic | 1 | 7 | 2 | .71 | .947 |
| Nonenhanced tumor | 4 | 4 | 2 | .66 | .932 |
| *IDH1* | | | | | |
| Edema | 1 | 0 | 0 | .60 | .932 |
| Contrast-enhanced tumor | 1 | 0 | 0 | .08 | .64 |
| Necrotic | 1 | 0 | 0 | .19 | .72 |
| Nonenhanced tumor | 0 | 0 | 1 | .23 | .72 |
| *NF1* | | | | | |
| Edema | 1 | 2 | 1 | .81 | >.99 |
| Contrast-enhanced tumor | 0 | 3 | 1 | >.99 | >.99 |
| Necrotic | 0 | 4 | 0 | .37 | .88 |
| Nonenhanced tumor | 2 | 2 | 0 | .67 | .932 |
| *PIK3CA* | | | | | |
| Edema | 0 | 0 | 1 | >.99 | >.99 |
| Contrast-enhanced tumor | 0 | 0 | 1 | .27 | .72 |
| Necrotic | 0 | 1 | 0 | >.99 | >.99 |
| Nonenhanced tumor | 1 | 0 | 0 | >.99 | >.99 |
| *PIK3R1* | | | | | |
| Edema | 1 | 0 | 2 | .77 | .986 |
| Contrast-enhanced tumor | 2 | 1 | 0 | .03 | .64 |
| Necrotic | 1 | 1 | 1 | .40 | .88 |
| Nonenhanced tumor | 0 | 1 | 2 | .08 | .64 |
| *PTEN* | | | | | |
| Edema | 4 | 6 | 4 | .44 | .88 |
| Contrast-enhanced tumor | 2 | 11 | 1 | .27 | .72 |
| Necrotic | 2 | 7 | 5 | .63 | .932 |
| Nonenhanced tumor | 7 | 4 | 3 | >.99 | >.99 |
| *RB1* | | | | | |
| Edema | 2 | 2 | 0 | .21 | .72 |
| Contrast-enhanced tumor | 1 | 3 | 0 | .43 | .88 |
| Necrotic | 0 | 2 | 2 | .49 | .923 |
| Nonenhanced tumor | 1 | 2 | 1 | .67 | .932 |
| *TP53* | | | | | |
| Edema | 2 | 5 | 2 | .21 | .72 |
| Contrast-enhanced tumor | 2 | 7 | 0 | .08 | .64 |
| Necrotic | 3 | 3 | 3 | .24 | .72 |
| Nonenhanced tumor | 2 | 4 | 3 | .27 | .72 |

.06 uncorrected), and none after false discovery rate correction.

## Discussion

Consistent with previous studies (7,8, 22,23), we detected a significant correlation between overall survival and the degree of contrast enhancement as well as the length of the major axis of the lesion. Of importance, we also noted that these imaging features were still strongly associated with overall survival even after adjusting for KPS, suggesting that these radiologist-made measurements of tumor size and composition may provide additional prognostic value on top of standard clinical variables. Currently, analyses comparing the abilities of these same imaging features in addition to standard clinical variables to predict overall survival to those of standard clinical variables are underway. While data are still being generated from additional cases, the initial findings connecting radiology, outcome, and genomics clearly demonstrate the power

**Table 4**

**Distribution of Copy Number Variation according to Neuroimaging Features and Association Analysis**

| Gene, Neuroimaging Feature, and Copy No. Variation | No. of Tumors with Copy No. Variation (Out of 47) according to Percentage of Total Abnormal Tissue | | | *P* Value (Fisher Exact Test) | Benjamini-Hochberg Corrected *P* Values |
|---|---|---|---|---|---|
| | 0%–5% | 6%–33% | 34%–95% | | |
| *CDKN2A* | | | | | |
| Edema | | | | | |
| Homozygous deletion | 4 | 7 | 8 | .65 | .975 |
| Normal | 9 | 7 | 11 | | |
| Contrast-enhanced tumor | | | | | |
| Homozygous deletion | 0 | 15 | 5 | .16 | .48 |
| Normal | 4 | 19 | 4 | | |
| Necrotic | | | | | |
| Homozygous deletion | 7 | 10 | 3 | .05 | .28 |
| Normal | 2 | 16 | 9 | | |
| Nonenhanced tumor | | | | | |
| Homozygous deletion | 9 | 5 | 6 | .74 | .987 |
| Normal | 14 | 8 | 5 | | |
| *EGFR* | | | | | |
| Edema | | | | | |
| Normal | 8 | 5 | 9 | .43 | |
| Amplification | 5 | 9 | 10 | | .975 |
| Contrast-enhanced tumor | | | | | |
| Normal | 4 | 13 | 5 | .06 | .28 |
| Amplification | 0 | 21 | 4 | | |
| Necrotic | | | | | |
| Normal | 4 | 9 | 9 | .07 | .28 |
| Amplification | 5 | 17 | 3 | | |
| Nonenhanced tumor | | | | | |
| Normal | 10 | 6 | 6 | .93 | >.99 |
| Amplification | 13 | 7 | 5 | | |
| *PDGFRA* | | | | | |
| Edema | | | | | |
| Normal | 12 | 12 | 17 | >.99 | >.99 |
| Amplification | 1 | 2 | 2 | | |
| Contrast-enhanced tumor | | | | | |
| Normal | 4 | 30 | 8 | >.99 | |
| Amplification | 0 | 4 | 1 | | >.99 |
| Necrotic | | | | | |
| Normal | 9 | 23 | 10 | .57 | |
| Amplification | 0 | 3 | 2 | | .975 |
| Nonenhanced tumor | | | | | |
| Normal | 19 | 12 | 11 | .49 | .975 |
| Amplification | 4 | 1 | 0 | | |

of this approach; of importance, we demonstrated that noninvasive, imaging-based features can be used as prognostic biomarkers.

The use of clinical and imaging features either alone or in conjunction with each other for prognosis is of course not a new area of research. Clinical characteristics that have emerged from recursive partitioning analysis and serve as the reference standard for predictive models in GBM include KPS, sex, and age (24). Our Cox regression analyses found contrast enhancement to be predictive of survival, consistent with earlier studies (8,23). Of note, however, in many earlier studies the estimations of contrast enhancement were not based on a standardized visual feature set, which suggests that our findings may be more robust.

Value of these data also lies with the integration and correlation of imaging features with the molecular data from this TCGA cohort. We observed that tumors classified as proneural demonstrated significantly less contrast

enhancement than other tumor types. Similarly, the mesenchymal subtype was noted to show consistently less nonenhancement than the other tumor subtypes. These results likely imply distinct growth properties of proneural and mesenchymal GBMs. Furthermore, tumors harboring *EGFR* mutations were significantly larger than *EGFR* wild-type tumors and *TP53* mutant GBMs were significantly smaller than *TP53* wild-type tumors. As a group, *EGFR* mutant GBMs were larger than *TP53* mutant tumors. We also found that *EGFR* copy number amplification was marginally correlated with both contrast-enhanced tumor volume and necrosis was correlated with deletion of *CDKN2A*. While *PIK3R1* was noted to have an association, the number of total events is so low that it is not informative. Although a number of correlations between genes that are frequently mutated in GBM and neuroimaging properties were noted, we caution that these associations must be considered preliminary due to the relatively small number of cases and also because none of these survived comparison for multiple corrections.

Other studies have attempted to develop radiogenomic phenotypes in gliomas. For example, Diehn et al (25) found that the imaging feature of mass effect (resulting from growing tumor pressing against other areas of the brain) was highly correlated to the genetic expression of genes involved in proliferation and cell-cycle progression. Likewise, similar methods were used to identify genes involved in blood-brain barrier maintenance, hypoxia, angiogenesis, and extracellular matrix remodeling owing to their upregulation in tumors with high contrast enhancement tumors compared with tumors with low contrast enhancement (5,26) A recent study by Zinn et al (9) used volumetric measurements of the TCGA data to demonstrate specific gene associations with edema volumes.

While our study represents a methodologic and radiogenomic advance, it has a number of limitations. First, we noted a relatively heterogeneous nature of gene-level mutations, such that only a small percentage of GBMs had mutations in a given gene. With greater numbers of cases for future studies, other genotype-phenotype correlations may be uncovered. Additionally, although necrosis has been previously shown to be associated with poorer outcome (7,8,27), it was not found to be a significant predictor in this study. It is possible that the percentage cutoffs used to define the groupings (eg, 0%–5%, 5%–33%) may not have been sensitive enough to detect this association. Similarly, we were unable to find a previously demonstrated association (5) between nonenhanced tumor and survival, an association Pope et al discovered by using univariable analyses. Also as discussed above, the observed correlations between copy number and mutation status did not survive comparison for multiple comparisons.

Collection and assessment of new GBM cases is still ongoing by our consortium, and with the relatively limited number of cases ($n$ = 75) and number of features in the full visual feature set ($n$ = 30), this initial study attempted to validate and assess whether the cardinal imaging features would be easily comparable to previous work (eg, proportion of necrosis, contrast enhancement, edema, nonenhanced tumor). This study only utilized a subset of the entire visual feature set, focusing on the semiquantitative assessments of the tumor compartments, and so does not address the reliability or reproducibility of the other features. Future work will include not only more quantitative assessments of tumor compartments by using volumetrics, but will also include metrics obtained from additional imaging modalities such as diffusion tensor and perfusion imaging.

For neuroimaging-based investigation, it is often challenging to extract objective information for scientific analysis from prose statements of imaging features by neuroradiologists who typically use idiosyncratic vocabulary. The results of our interrater assessment suggest that use of a consistent or controlled set of imaging features can substantially address concerns regarding validation and reproducibility of imaging-centric correlative research. These radiogenomic results support the theme that the phenotypic properties of a brain tumor visualized at MR imaging has the power to provide insight into the genetic and molecular properties of the tumors. These associations have important implications and could eventually assist neuroradiologists in subtyping tumors based on imaging phenotype. Moreover, what is yet to be determined is if consideration of tumor-specific imaging features can be successfully mobilized to more effectively guide therapeutic decisions for individual patients.

**Disclosures of Conflicts of Interest: D.A.G.** No relevant conflicts of interest to disclose. **L.A.D.C.** No relevant conflicts of interest to disclose. **S.N.H.** No relevant conflicts of interest to disclose. **C.A.H.** No relevant conflicts of interest to disclose. **J.J.G.** No relevant conflicts of interest to disclose. **T.D.A.** No relevant conflicts of interest to disclose. **W.D.D.** No relevant conflicts of interest to disclose. **L.S.** No relevant conflicts of interest to disclose. **T.M.** No relevant conflicts of interest to disclose. **R.J.** No relevant conflicts of interest to disclose. **M.W.** Financial activities related to the present article: none to disclose. Financial activities not related to the present article: grants to institution from GE Healthcare and Philips Healthcare. Other relationships: none to disclose. **M.J.** No relevant conflicts of interest to disclose. **P.R.** No relevant conflicts of interest to disclose. **E.H.** Financial activities related to the present article: none to disclose. Financial activities not related to the present article: former stockholder GE and Johnson and Johnson. Other relationships: none to disclose. **R.J.C.** No relevant conflicts of interest to disclose. **P.M.** No relevant conflicts of interest to disclose. **V.K.** No relevant conflicts of interest to disclose. **J.F.** No relevant conflicts of interest to disclose. **J.K.** No relevant conflicts of interest to disclose. **P.O.Z.** No relevant conflicts of interest to disclose. **C.S.M.** No relevant conflicts of interest to disclose. **C.J.** No relevant conflicts of interest to disclose. **R.C.** No relevant conflicts of interest to disclose. **D.R.** Financial activities related to the present article: none to disclose. Financial activities not related to the present article: instution grants from GE Medical Systems. Other relationships: none to disclose. **J.S.** Financial activities related to the present article: none to disclose. Financial activities not related to the present article: Board membership, Appistry; consultancy, Ceadars-Sinai; stock/stock options, Appistry. Other relationships: none to disclose. **A.F.** Financial activities related to the present article: none to disclose. Financial activities not related to the present article: textbook royalties from LWW. Other relationships: none to disclose. **D.J.B.** No relevant conflicts of interest to disclose.

## References


1. Louis DN, Ohgaki H, Wiestler OD, Cavenee WK. WHO classification of tumours of the central nervous system. 4th ed. Lyon, France: International Agency for Research, 2007.
2. Central Brain Tumor Registry of the United States. CBTRUS statistical report: primary brain and central nervous system tumors in the United States in 2004–2006. Hinsdale, Ill: Central Brain Tumor Registry of the United States, 2010.
3. Stupp R, Mason WP, van den Bent MJ, et al. Radiotherapy plus concomitant and adjuvant temozolomide for glioblastoma. N Engl J Med 2005;352(10):987–996.
4. Bonavia R, Inda MM, Cavenee WK, Furnari FB. Heterogeneity maintenance in glioblastoma: a social network. Cancer Res 2011;71(12):4055–4060.
5. Pope WB, Sayre J, Perlina A, Villablanca JP, Mischel PS, Cloughesy TF. MR imaging correlates of survival in patients with high-grade gliomas. AJNR Am J Neuroradiol 2005;26(10):2466–2474.
6. Park JK, Hodges T, Arko L, et al. Scale to predict survival after surgery for recurrent glioblastoma multiforme. J Clin Oncol 2010;28(24):3838–3843.
7. Lacroix M, Abi-Said D, Fourney DR, et al. A multivariate analysis of 416 patients with glioblastoma multiforme: prognosis, extent of resection, and survival. J Neurosurg 2001;95(2):190–198.
8. Hammoud MA, Sawaya R, Shi W, Thall PF, Leeds NE. Prognostic significance of preoperative MRI scans in glioblastoma multiforme. J Neurooncol 1996;27(1):65–73.
9. Zinn PO, Mahajan B, Sathyan P, et al. Radiogenomic mapping of edema/cellular invasion MRI-phenotypes in glioblastoma multiforme. PLoS ONE 2011;6(10):e25451.
10. Wiki for the VASARI feature set. The National Cancer Institute Web site. https://wiki.cancerimagingarchive.net/display/Public/VASARI+Research+Project. Updated May 25, 2012.
11. The Cancer Imaging Archive (TCIA). The National Cancer Institute Web site. http://cancerimagingarchive.net/. Accessed December 21, 2011.
12. Cancer Biomedical Informatics Grid. Clearcanvas with the AIM plugin. National Cancer Institute Web site. https://gforge.nci.nih.gov. Accessed December 28, 2011.
13. New AS, Hazlett EA, Newmark RE, et al. Laboratory induced aggression: a positron emission tomography study of aggressive individuals with borderline personality disorder. Biol Psychiatry 2009;66(12):1107–1114.
14. Channin DS, Mongkolwat P, Kleper V, Rubin DL. The annotation and image mark-up project. Radiology 2009;253(3):590–592.
15. Channin DS, Mongkolwat P, Kleper V, Sepukar K, Rubin DL. The caBIG annotation and image markup project. J Digit Imaging 2010;23(2):217–225.
16. Rubin DL, Mongkolwat P, Channin DS. A semantic image annotation model to enable integrative translational research. Summit on Translat Bioinforma 2009;2009:106–110.
17. Krippendorff K. Computing Krippendorf's Alpha-Reliability. http://repository.upenn.edu/asc_papers/43/. Published 2011. Accessed December 12, 2011.
18. Verhaak RG, Hoadley KA, Purdom E, et al. Integrated genomic analysis identifies clinically relevant subtypes of glioblastoma characterized by abnormalities in PDGFRA, IDH1, EGFR, and NF1. Cancer Cell 2010;17(1):98–110.
19. Phillips HS, Kharbanda S, Chen R, et al. Molecular subclasses of high-grade glioma predict prognosis, delineate a pattern of disease progression, and resemble stages in neurogenesis. Cancer Cell 2006;9(3):157–173.
20. Benjamini Y, Hochberg Y. Controlling the false discovery rate: a practical and powerful approach to multiple testing. J R Stat Soc Ser A Stat Soc 1995;57(1):289–300.
21. cBio Cancer Genomics Portal. Memorial Sloan-Kettering Cancer Center Web site. http://www.cbioportal.org/public-portal/. Updated May 9, 2012.
22. Garzón B, Emblem KE, Mouridsen K, et al. Multiparametric analysis of magnetic resonance images for glioma grading and patient survival time prediction. Acta Radiol 2011;52(9):1052–1060.
23. Chaichana KL, Kosztowski T, Niranjan A, et al. Prognostic significance of contrast-enhancing anaplastic astrocytomas in adults. J Neurosurg 2010;113(2):286–292.
24. Curran WJ Jr, Scott CB, Horton J, et al. Recursive partitioning analysis of prognostic factors in three Radiation Therapy Oncology Group malignant glioma trials. J Natl Cancer Inst 1993;85(9):704–710.
25. Diehn M, Nardini C, Wang DS, et al. Identification of noninvasive imaging surrogates for brain tumor gene-expression modules. Proc Natl Acad Sci U S A 2008;105(13):5213–5218.
26. Pope WB, Chen JH, Dong J, et al. Relationship between gene expression and enhancement in glioblastoma multiforme: exploratory DNA microarray analysis. Radiology 2008;249(1):268–277.
27. Barker FG 2nd, Davis RL, Chang SM, Prados MD. Necrosis as a prognostic factor in glioblastoma multiforme. Cancer 1996;77(6):1161–1166.